Materials Advances

ROYAL SOCIETY OF CHEMISTRY

PAPER

View Article Online
View Journal | View Issue

Cite this: *Mater. Adv.*, 2026, 7, 2785

Sustainable removal of brilliant green dye from aqueous media using a calcium alginate–polydopamine bio-composite: process optimization and adsorption mechanism

Marwa Magdy,[a] Mohamed M. Aboelnga [ab] and Elsayed Elbayoumy *[a]

The contamination of water with toxic dyes poses serious threats to both aquatic environments and human health. The present study demonstrates a bio-polymer composite of calcium alginate with polydopamine (Ca-alginate/PDA), which was prepared and tested as an effective adsorbent material for brilliant green dye (BG) removal from aqueous solution. The successful formation and structure properties of the Ca-alginate/PDA composite were confirmed *via* different characterization techniques, including XRD, XPS, FTIR, BET, and FESEM, exhibiting a large surface area of 131.59 m^2 g^{-1}. Batch adsorption experiments identified the optimal operating conditions for dye removal to be pH 5.7, a temperature of 298 K, an adsorbent dosage of 0.1 g, an initial concentration of dye of 7 mg L^{-1}, and a contact time of 75 minutes, under which the maximum removal efficiency of 99.07% was achieved. Isotherm analysis revealed good correlation with the Freundlich isotherm, indicating that the multilayer adsorption occurred on a heterogeneous surface, but the kinetic analysis followed the pseudo-first-order kinetic model. Also, the thermodynamic study indicated the endothermic (positive ΔH) and spontaneous (negative ΔG) nature of the process. The mechanisms of adsorption were identified as $\pi-\pi$ interactions, electrostatic interactions and hydrogen bond interactions. Moreover, regeneration tests showed that poly(dopamine)/Ca-alginate retained high efficiency and stability across four reuse cycles. Optimization using Box–Behnken design provided a reliable statistical model to predict the behavior of adsorption under various parameters. Overall, this study demonstrates the potential of poly(dopamine)/Ca-alginate as a durable and highly effective adsorbent for removing dye (BG) from wastewater.

Received 16th November 2025,
Accepted 24th January 2026

DOI: 10.1039/d5ma01333j

rsc.li/materials-advances

1. Introduction

Water pollution resulting from the uncontrolled release of industrial effluents, including synthetic dyes, oils and heavy metals, and into aquatic systems has become a serious global issue affecting both the environment and public health.[1–4] Among these pollutants, synthetic dyes are particularly problematic due to their extensive use in the textile, printing, plastics, leather, and cosmetics industries, as well as their chemical stability, toxicity, and resistance to natural biodegradation processes.[5–8] Dye contamination in water bodies not only impedes light penetration, thereby disrupting photosynthesis and threatening aquatic ecosystems, but also reduces gas solubility, limiting re-oxygenation and ultimately leading to anaerobic conditions.[9–11]

The dye of BG is a synthetic cationic dye, which is utilized in different industries, for example wool, rubber, silk, leather and paper processing, as well as in pharmaceutical formulations and veterinary medicine.[12–15] Even at trace concentrations, BG dye imparts intense coloration, inhibits photosynthetic activity, and poses risks to aquatic organisms and human health.[16] Consequently, developing efficient, cost-effective, and environmentally sustainable approaches for eliminating such dyes from wastewater is of great importance.

Numerous physicochemical and biological techniques have been used for removing dyes, including oxidation, coagulation, membrane filtration, microbial degradation, photocatalysis, adsorption, and electrochemical processes.[17–19] Among these, adsorption has emerged as one of the most efficient and economically viable approaches owing to its ease of operation, high efficiency, and reusability.[20–22] A diverse range of adsorbents have been reported, including activated carbon, porous solids, graphene-based materials, metal–organic frameworks,

[a] *Chemistry Department, Faculty of Science, Damietta University, New Damietta, 34517, Egypt. E-mail: marwasleem@du.edu.eg, Mohamed.aboelnga@du.edu.eg, sayedelbayoumy@du.edu.eg*
[b] *King Salman International University, Faculty of Basic Sciences, Ras Sudr, 46612, South Sinai, Egypt*

biomaterials, nanoparticles, clay minerals, and polymeric matrices.[23,24] Polymeric materials have shown great promise as adsorbents for both inorganic and organic contaminations due to their tunable structure, surface chemistry, and ease of processing.[25–30] For instance, poly(AN-*co*-AMPS),[31] poly(divinylbenzene) (polyDVB),[32] amine-modified tannin gel (ATG), and magnetic barium phosphate composites[33] have been reported for BG dye removal. Furthermore, hybrid polymeric adsorbents such as NiO/polydopamine nanocomposites,[34] calcium alginate beads,[35] and polydopamine/silver nanoparticles[36] have demonstrated excellent potential for wastewater treatment applications. In addition to these materials, hydrogel-based adsorbents have attracted considerable attention for dye removal due to their three-dimensional crosslinked networks, high water uptake, and abundant functional groups. Different polymeric hydrogels, such as sodium alginate-*g*-poly(acrylamide-clay)/TiO_2 hydrogel nanocomposite [SA-*g*-p(AM–Bn)/TiO_2], gum acacia-cl-acrylic acid-*co*-itaconic acid (GA-cl-AA-*co*-IA) hydrogels, chitosan/hematite nano-composite hydrogel capsules (HC–H), and terpolymer biocomposite hydrogel poly(CMC-*co*-AM-*co*-ITA)/AC, have been widely reported for the efficient adsorption of different dyes.[37–44]

Natural biopolymers such as alginate are of particular interest due to their inherent biodegradability, cost-effectiveness, and environmentally friendly properties, which make them ideal for sustainable water treatment.[45] In parallel, polydopamine (PDA), a mussel inspired polymer formed through oxidative self-polymerization of dopamine, has gained increasing attention as a versatile coating and adsorbent material. PDA exhibits strong adhesion to diverse substrates, remarkable chemical stability and higher density of amino groups and phenolic hydroxyl, which make it suitable for adsorption-based pollutant removal and water purification.[46]

In this context, polymeric composites based on calcium alginate and PDA have emerged as highly promising adsorbents. The synergistic properties of these two components combine the porous, negatively charged alginate matrix that favors electrostatic interactions with cationic dyes like BG, and the catechol/amine-rich PDA that enables hydrogen bonding, π–π stacking, and coordination interactions.[47] Moreover, integration of PDA enhances the surface area, stability, and reusability, yielding a biocompatible and environmentally friendly adsorbent with superior dye removal capacity.

In the present study, a calcium alginate–polydopamine (Ca-alginate/PDA) polymeric composite was synthesized and systematically evaluated as a green adsorbent for the removal of brilliant green (BG) dye from aqueous media. The novelty of this work lies in the integration of material design, mechanistic understanding, and statistical optimization, which has not been comprehensively reported for BG adsorption. The composite exhibits a high surface area, diverse functional groups, and a porous structure, enabling efficient adsorption through electrostatic interactions, hydrogen bonding, and π–π stacking. The physicochemical properties of the hydrogel were thoroughly characterized, and the effects of key operational parameters on adsorption performance were investigated. Adsorption behavior was analyzed using isotherm, kinetic, and thermodynamic models, while a Box–Behnken design was employed for process optimization. Furthermore, a regeneration study assessed the reusability of the composite under repeated cycles. Overall, this work provides a sustainable and efficient approach for BG dye removal, combining structural design, mechanistic insight, and optimization to advance the application of Ca-alginate/PDA hydrogels in wastewater treatment.

2. Materials and methods

2.1. Materials

Dopamine hydrochloride (98%) was purchased from Sigma-Aldrich (USA). Sodium alginate was sourced from Belami Fine Chemicals Pvt. Ltd (India). Ethanol (analytical reagent grade, >99.7%) and aqueous ammonia solution (28–30%) were supplied by Scharlau Chemical Reagents (Spain). Calcium chloride ($CaCl_2$), potassium nitrate (KNO_3), sodium hydroxide (NaOH) and hydrochloric acid (HCL) were procured from Fisher Scientific (UK). Brilliant green (BG) dye was purchased by Aldrich Chemicals (USA). Distilled water was used as the solvent in all experiments. All chemicals were used in their original form without additional purification.

2.2. Synthesis of polydopamine

Polydopamine (PDA) was synthesized according to the procedure described by Liu *et al.*[48] using an alcohol–water mixed solvent. Briefly, ethanol (36 mL) was combined with aqueous ammonia (0.84 mL, 28–30%) and diluted to 120 mL with deionized water. The solution was stirred (400 rpm) for 30 min at room temperature. Subsequently, a dopamine hydrochloride solution (0.45 g in 9 mL deionized water) was added, resulting in a color change from pale brown to dark brown. The reaction continued for 48 hours. The resulting PDA was collected using centrifugation (6000 rpm, 10 min), washed repeatedly with deionized water, dried under vacuum, and saved for further use.

2.3. Preparation of the calcium alginate/polydopamine composite

The calcium alginate/polydopamine (Ca-alginate/PDA) composite was prepared following a modified version of the method described in a previous report.[49] Briefly, sodium alginate (0.5 g) and polydopamine (0.5 g) were separately dissolved in deionized water (50 mL) to ensure complete dispersion. Then the two solutions were combined and mechanically stirred (800 rpm) to yield a uniform solution. This mixture was introduced dropwise into 100 mL of a 3% (w/v) $CaCl_2$ solution using a syringe, allowing the calcium ions to initiate ionic crosslinking of the alginate chains while simultaneously embedding PDA within the polymeric network. The formed hydrogel beads were gently agitated for 2 hours to ensure complete gelation, rinsed overnight thoroughly with deionized water to remove residual Ca^{2+} ions, and subsequently vacuum drying at 40 °C overnight.

2.4. Characterization techniques

The FTIR spectra were recorded using a JASCO FT/IR-6100 spectrometer in the range of 4000–400 cm^{-1} by using KBr pellet samples. Using a 200 kV accelerating voltage with a JEM-2100F microscope, a field emission scanning electron microscopy image was produced. The Brunauer–Emmett–Teller (BET) technique was employed to calculate the pore volume and surface area and through nitrogen sorption measurements through a Quantachrome analyzer. To examine the particle size and crystalline structure of the polymer composite, the analysis of wide-angle X-ray diffraction (XRD) was carried out on a Siemens *D*-500 diffractometer (λ = 1.54 Å, Cu Kα). X-ray photoelectron spectroscopy (XPS) was performed using a Kratos AXIS Ultra DLD spectrometer equipped with a monochromatic Al Kα radiation source ($h\nu$ = 1486.6 eV). Both survey and high-resolution spectra were obtained under ultra-high vacuum conditions to identify the chemical states and elemental composition on the surface of the sample, with the binding energy scale calibrated against the C 1s peak at 284.8 eV. A Jasco V-630 UV-visible spectrophotometer was used to record the UV-vis absorption spectra that were measured by employing a quartz cell (1 cm) and a wavelength range from 250–500 nm at room temperature.

2.5. Batch adsorption experiments

The experiments of batch adsorption were carried out to examine the influence of different operational parameters such as time (0–120), temperature (298–328 K), amount of adsorbent (0.01–0.07 g), initial BG concentration (7–14.6 mg L^{-1}) and pH (3–9) on the BG dye adsorption by Ca-alginate/PDA. A fixed quantity of adsorbent was added to 100 ml of BG dye solution with a specific concentration, and the pH was adjusted using HCl or NaOH as required. Then, the solution was shaken for 120 min at 250 rpm in the shaker, after adding a known quantity of adsorbent. Then, the solution of BG dye was centrifuged, and the residual concentration of dye at equilibrium (C_e) was determined using a UV-vis spectrophotometer at λ = 625 nm. To ensure greater accuracy, each experiment was conducted three times. The removal efficiency (*R*%) and adsorption capacity (q_t) of BG dye adsorbed by Ca-alginate/PDA at time t were calculated using the eqn (1) and (2), respectively.[50,51]

$$\%(R) = \frac{C_0 - C_t}{C_0} \times 100 \quad (1)$$

$$q_t = \frac{C_0 - C_t}{W} \times V \quad (2)$$

where C_t is the residual dye concentration at time t (mg L^{-1}), C_0 is the BG dye initial concentration (mg L^{-1}), V is the volume of the solution of BG dye (L) and W is the amount of (Ca-alginate/PDA) (g).

2.6. Recycling experiments

The ability to regenerate the adsorbent helps lower material costs, which is a significant economic advantage. The regeneration performance of Ca-alginate/PDA was evaluated through a series of adsorption/desorption experiments.[52] Initially, 100 mg of Ca-alginate/PDA was used to adsorb BG dye from 100 mL of 7.5 mg L^{-1} dye solution over a 60-minute period. After the adsorption step, the Ca-alginate/PDA-dye was separated by using the centrifuge and treated with 100 mL of a 0.5 mol L^{-1} HCl solution for 60 minutes. Then the regenerated polymer was collected through centrifugation, thoroughly rinsed with distilled water and dried overnight for 24 hours in an oven. The dye-free Ca-alginate/PDA obtained was reused in a subsequent adsorption cycle.

3. Results and discussion

3.1. Adsorbent characterization

3.1.1. FTIR analysis. The FTIR spectra of the Ca-alginate/PDA composite before and after BG dye adsorption are presented in Fig. 1a. The pristine composite exhibits a broad band in the range 3600 to 3200 cm^{-1} (3578, 3518, and 3314 cm^{-1}), related to O–H stretching vibrations (from alginate hydroxyl and PDA phenolic groups) and N–H (from PDA amine groups). Characteristic absorption bands of alginate are observed at 1594 cm^{-1} and 1415 cm^{-1}, attributed to the symmetric and asymmetric stretching vibrations of carboxylate groups ($-COO^-$), respectively. The bands at 1081 and 1029 cm^{-1} are associated with C–O–C and C–O vibrations of the glycosidic backbone, while PDA contributes additional aromatic C=C and C–N modes in the 1600–1500 cm^{-1} region. After BG adsorption, significant spectral changes are evident: the O–H/N–H stretching region becomes less intense, indicating hydrogen bonding between BG molecules and PDA/alginate functional groups; the carboxylate bands shift (ν_as(COO^-) from 1594–1531 cm^{-1} and ν_s(COO^-) from 1415–1427 cm^{-1}), confirming strong electrostatic interactions between the anionic carboxyl groups of alginate and the cationic BG dye; and modifications in the aromatic region reflect π–π stacking and charge-transfer interactions between PDA's catechol/indole-like structures and the conjugated aromatic rings of BG. Minor perturbations in the C–O stretching bands further suggest structural rearrangements in the alginate matrix upon dye uptake. Collectively, these results confirm that BG adsorption onto Ca-alginate/PDA is governed primarily by π–π stacking, hydrogen bonding and electrostatic attraction.[53–55]

3.1.2. X-ray photoelectron spectroscopy (XPS) analysis. XPS analysis was used to investigate the elemental states and the chemical composition of the surface for the synthesized Ca-alginate/PDA. The wide scan survey spectrum (Fig. 1f) confirms the presence of four main elements: carbon C 1s, nitrogen N 1s, oxygen O 1s, and calcium (Ca 2p) at 284.9, 532.2, 399.2, and 347.7 eV, respectively, which are characteristic elements for the biopolymer composite. Also, the chemical composition (in weight percentage %) of Ca-alginate/PDA was found to be 26.74 for oxygen, 65.97 for carbon, 4.6 for nitrogen and 1.97 for calcium. The high-resolution spectrum of each element offers valuable information about the specific functional

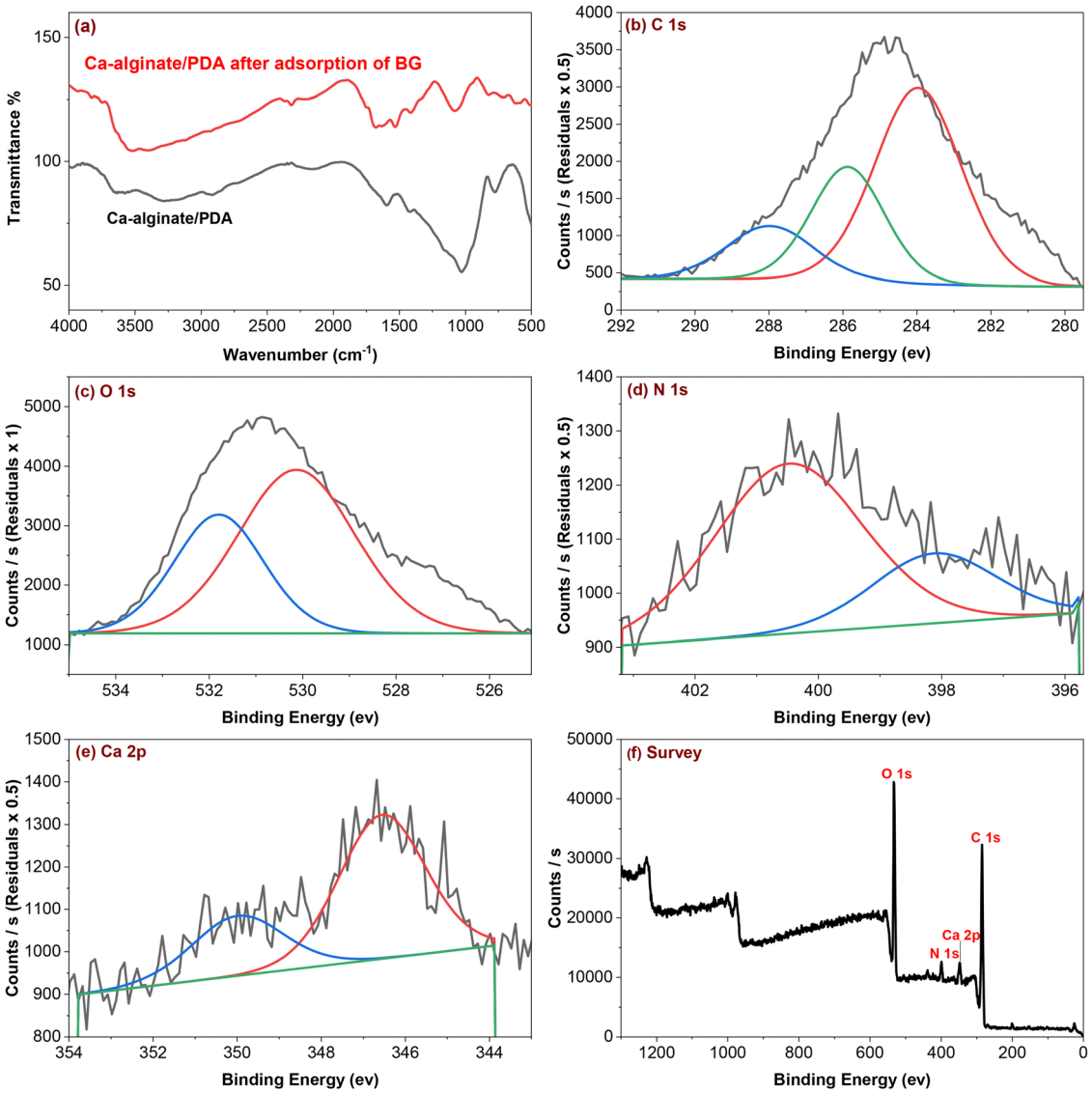

Fig. 1 FTIR spectra of Ca-alginate/PDA before and after the adsorption process (a); XPS analysis of Ca-alginate/PDA: (b) high-resolution C 1s spectrum, (c) high-resolution O 1s spectrum, (d) high-resolution N 1s spectrum, (e) high-resolution Ca 2p spectrum, and (f) the presence of O, C, N, and Ca elements in the Ca-alginate/PDA indicated by survey.

groups within the material. The spectrum of C 1s (Fig. 1b) displays three main peaks at 284.75 eV, 287.65 eV, and 282.15 eV, assigned to C–C/C═C, C═O/O–C═O, and C═N functional groups, respectively, which are characteristics of both alginate and the dopamine backbone.[56] The N 1s spectrum (Fig. 1d) displays two peaks at 400.17 eV and 397.08 eV, which correspond to –NH– and C═N groups.[57] The O 1s spectrum (Fig. 1c) showed two peaks at 530.23 and 531.81 eV. The peak at 530.23 eV corresponds to the oxygen atoms in metal–oxygen bonds (Ca–O) in calcium alginate, or possibly C═O in carboxyl groups, while the other peak at 531.81 eV is typically associated with C–O bonds (alcohol, phenolic –OH) and C–O–C bonds present in alginate and polydopamine.[58] The Ca 2p spectrum (Fig. 1e) shows two characteristic peaks at 346.55 eV and at 349.99 eV. These peaks are related to O–Ca bond and are indicative of Ca^{2+} in ionic coordination, most likely in the form of calcium alginate complexes.[59] Altogether, the results of XPS confirm the successful formation of Ca-alginate/PDA.

3.1.3. X-ray diffraction analysis. The crystalline characteristics of the prepared Ca-alginate/PDA composite were examined using XRD analysis, and the results are represented in Fig. 2a. The pattern of XRD exhibits a single broad diffraction peak centered at 2θ = 21.48°, which can be ascribed to the combined contributions of alginate and polydopamine. The broadness of this peak indicates the predominantly amorphous nature of the Ca-alginate/PDA composite, consistent with previous reports.[60]

3.1.4. Brunauer Emmett–Teller analysis. The specific surface area and pore structure of the synthesized Ca-alginate/PDA composite were evaluated through Brunauer–Emmett–Teller analysis at 77 K by employing nitrogen adsorption–desorption measurements. The resulting isotherm is presented

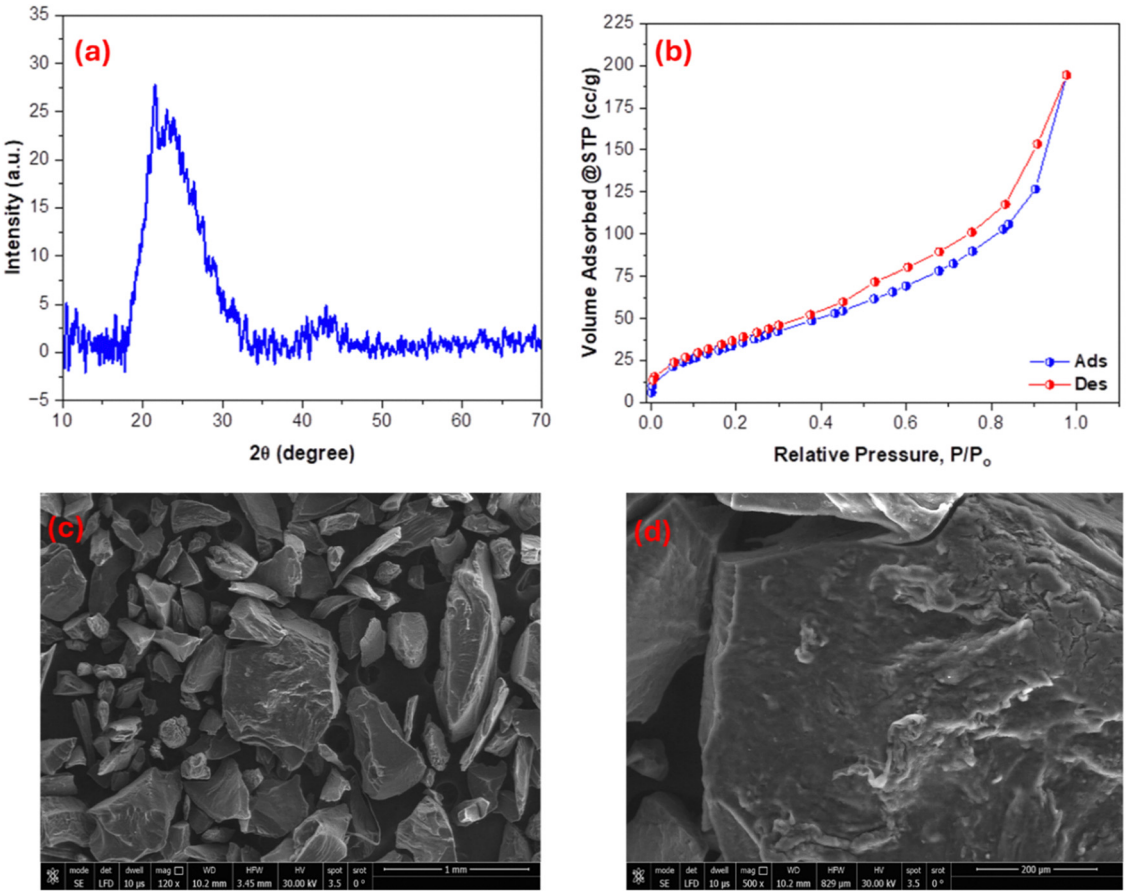

Fig. 2 XRD analysis (a); BET analysis (b); FESEM images with different scales, 1 mm (c) and 200 μm (d), of Ca-alginate/PDA.

in Fig. 2b. The composite exhibited a large specific surface area of 131.60 $m^2\ g^{-1}$ and the adsorption/desorption curve fits a type-V isotherm. Barrett–Joyner–Halenda (BJH) analysis additionally indicated the average pore radius of 1.985 nm and total pore volume of 0.281 $cm^3\ g^{-1}$ at saturation pressure. According to the International Union of Pure and Applied Chemistry (IUPAC) classification, pores are categorized as macropores (>50 nm), mesopores (2 to 50 nm), and micropores (<2 nm).[61,62] Based on this classification, the Ca-alginate/PDA composite falls within the microporous range. The relatively high specific surface area compared to other reported polymer-based adsorbents[31,63] is expected to enhance its adsorption capacity, providing more active sites for BG dye removal.

3.1.5. Field emission scanning electron microscopy (FESEM) analysis. The surface morphology of the synthesized Ca-alginate/PDA composite was examined using (FESEM) analysis, with the represented images presented in Fig. 2c and d. The FESEM micrographs at various magnifications reveal that the surface of the Ca-alginate/PDA composite is rough, irregular and composed of various sized and shaped particles. The observed morphology indicates that the presence of a porous framework, which has advantages for adsorption processes because it increases the surface area, offers more active sites for interaction of the dye and thereby improves its efficiency in removing pollutants like BG dyes from wastewater.

3.2. Swelling behavior of Ca-alginate/PDA

The swelling behavior of the Ca-alginate/PDA was evaluated to assess the water uptake capacity and integrity of the polymer network, which are important parameters for adsorption performance. The swelling percentage (%) was calculated using the following equation:

$$\text{Swelling percentage } (\%) = \frac{W_{\text{swollen}} - W_{\text{dry}}}{W_{\text{dry}}} \times 100$$

where W_{swollen} is the weight of the hydrogel after immersion in water and W_{dry} is the initial dry weight of Ca-alginate/PDA. The calculated swelling percentage value was found to be equal to 268%, indicating that the Ca-alginate/PDA network is sufficiently hydrated to facilitate diffusion of dye molecules while maintaining structural stability. This moderate swelling reflects a balanced network crosslinking and flexibility, which allows access to adsorption sites without compromising the mechanical integrity of the hydrogel.

3.3. Adsorption batch experiment

3.3.1. Point of zero charge (PZC). PZC is defined as the pH at which an adsorbent surface carries no net charge of an adsorbent. Accurate determination of the PZC is crucial for elucidating adsorption mechanisms, since electrostatic

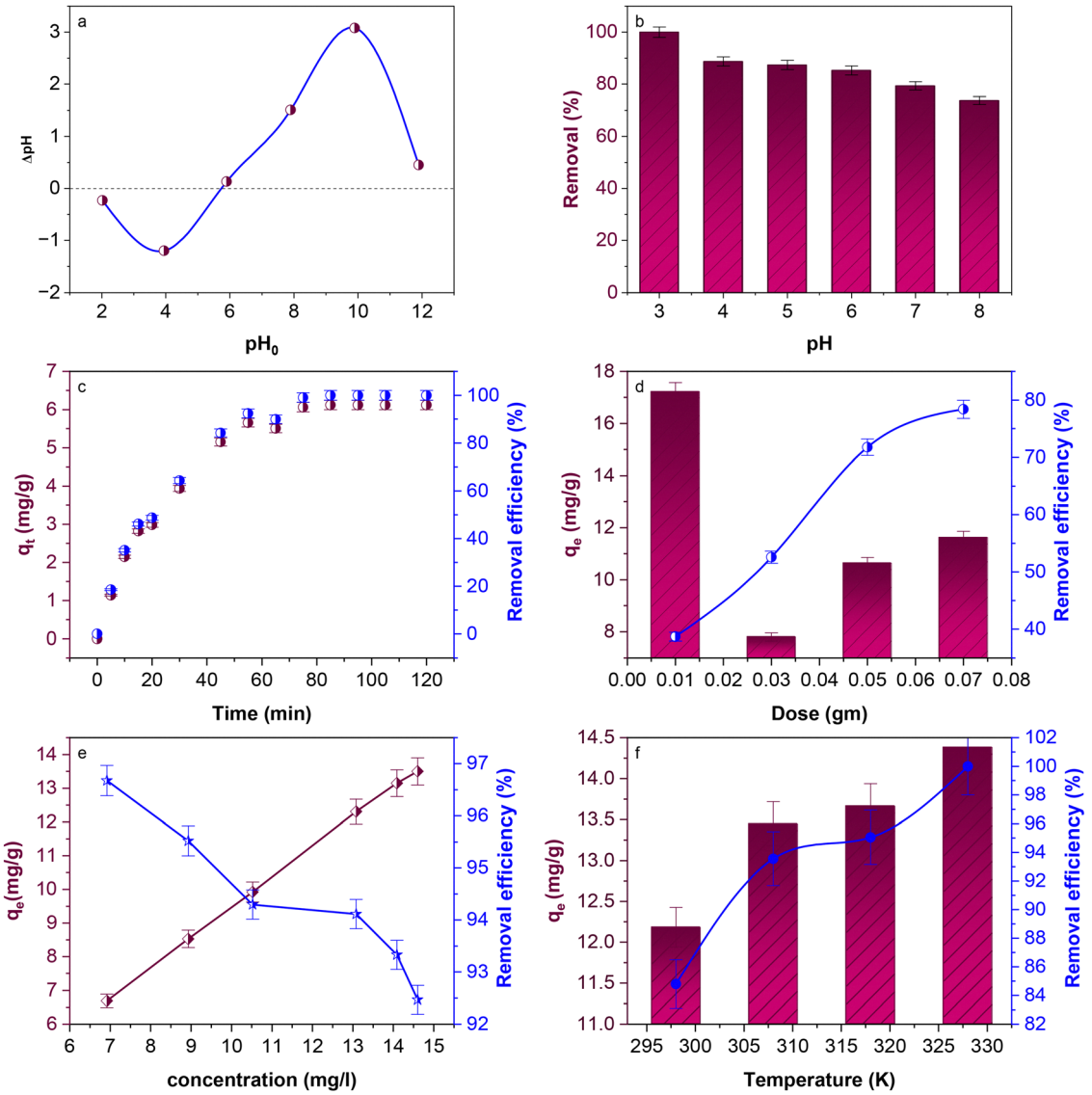

Fig. 3 (a) Point of zero charge; (b) influence of pH; (c) influence of contact time; (d) influence of adsorbent dose; (e) influence of dye concentration; (f) influence of temperature on adsorption process. Conditions of the adsorption: (b) pH (3–9), time = 60 min, 7 ppm initial concentration of dye, dose 0.1 g/100 ml and 298 K; (c) time (0–120 min), 7 ppm initial concentration of dye, pH equal to 5.7, dose 0.1 g/100 ml and 298 K; (d) dose (0.01–0.07 g)/100 ml, initial concentration of dye 8.9 ppm, pH equal to 5.7, 298 K and time 60 min; (e) initial concentration of dye (7–14.6 ppm), dosage 0.01 g/10 ml, pH equal to 5.7, 298 K and 120 min contact time; (f) temperature (298–328 K), pH = 5.74, initial concentration of dye = 14 ppm, dosage = 0.01 g/10 ml and 60 min contact time.

interactions between the adsorbent and solutes are strongly pH dependent. PZC of the Ca-alginate/PDA composite was evaluated using the pH drift method in 0.1 M KNO_3 solutions (pH 3 to 9), with adjustments made using 0.1 M NaOH and HCl. Following equilibration of 0.02 g of the composite with each solution for 48 h at ambient temperature, after which the values of pH were recorded from the intersection of initial and final pH values (Fig. 3a), the PZC was determined to be 5.7. At pH < 5.7, the composite surface acquires a net positive charge, thereby electrostatically facilitating the uptake of anionic species (*e.g.*, sulfonated dyes, oxyanions). Conversely, at pH > 5.7, the surface charge shifts to negative, thereby enhancing electrostatic affinity toward cationic pollutants such as metal cations and cationic dyes.[32]

3.3.2. Effect of pH. The BG dye adsorption on the Ca-alginate/PDA composite was strongly pH-dependent (Fig. 3b). Maximum removal (100%) occurred at pH 3, after which adsorption efficiency gradually decreased with increasing pH. Although the composite surface is positively charged below its PZC (5.7), high uptake under acidic conditions suggests that non-electrostatic interactions, for example hydrogen bonding and π–π stacking between dye molecule and PDA moieties, play a dominant role in driving adsorption under these conditions.[64–66] In addition, we observed that the color intensity of the BG dye decreases at low pH,[3,4] which reduces the amount of dye detected by the UV-vis spectrophotometer and consequently results in an apparently higher removal percentage under these acidic conditions. On the other hand, at

pH > 5.7, where the surface is negatively charged and expected to favor cationic dye adsorption, the removal efficiency decreased, likely due to competition with OH^- ions, reduced hydrogen bonding capacity, and dye aggregation.[64] These results highlight that adsorption is influenced by both electrostatic and non-electrostatic forces, with acidic conditions being most favorable.

3.3.3. Effect of contact time. The effect of time on adsorption of BG dye using the Ca-alginate/PDA composite was investigated over a time range of 5–120 min while keeping other experimental conditions constant, and the results are presented in Fig. 3c. As shown, both removal efficiency (R%) and adsorption capacity (q_e) increased rapidly with contact time, reaching a plateau after approximately 75 min, beyond which marginal improvements were observed until equilibrium was attained. The rapid adsorption rate at the beginning is related to the large number of readily available active binding sites on the composite surface. As contact time increased, the rate of dye uptake decreased, which is ascribed to progressive saturation of the available sites and the development of repulsive interactions between adsorbed dye molecules and those remaining in solution. Consequently, the adsorption process gradually approached equilibrium, at which point the number of dye molecules desorbing from the surface equaled those being adsorbed.[67,68]

3.3.4. Effect of adsorbent dose. The influence of Ca-alginate/PDA composite dose on adsorption of BG dye was examined by varying the amount of adsorbent between 0.01 and 0.07 g, with the other experimental conditions kept constant. As presented in Fig. 3d, the efficiency of removal rose from 38.7% to 78.4% with increasing adsorbent dose. This enhancement may be due to greater surface area and a larger number of active functional sites made available by the higher composite amount, which facilitates more effective interaction with dye molecules.[69] In contrast, the adsorption capacity (q_e) decreased from 3.4 to 0.99 mg g^{-1} as the adsorbent dose increased. This decline is commonly ascribed to the reduced adsorbate-to-adsorbent ratio at higher dosages, which leads to incomplete utilization of active sites and possible overlapping or aggregation of adsorbent particles, thereby lowering the efficiency per unit mass.[70] These findings are consistent with previous studies on dye adsorption, where an increase in adsorbent dosage improves the overall removal efficiency but results in a corresponding decrease in q_e due to unsaturated adsorption sites and reduced driving force for mass transfer.[69,70]

3.3.5. Effect of the concentration of dye. The influence of BG dye concentration on the adsorption performance was investigated over a range of 7.0–14.6 mg L^{-1}, with all other parameters held constant. As depicted in Fig. 3e, increasing the initial concentration of BG dye led to a slight reduction in removal efficiency from 96.7% to 92.5%. This reduction is due to the saturation of active adsorption sites at elevated solute concentrations, which means that more dye molecules remain unadsorbed in the solution.[71,72] In contrast, the adsorption capacity (q_e) improved significantly, rising from 6.69 to 13.5 mg g^{-1} as the initial BG dye concentration increased. This enhancement is driven by the enhanced mass transfer driving force and the higher collision frequency between dye molecules and adsorbent sites at greater concentrations.[73,74]

3.3.6. Effect of adsorption temperature. Temperature plays a vital role in the process of adsorption, as it influences both the interaction between adsorbate and adsorbent as well as the diffusion kinetics of solute molecules. The influence of temperature on BG dye adsorption using the Ca-alginate/PDA composite was investigated within the range of 298–328 K, with all other parameters kept constant. As illustrated in Fig. 3f, the adsorption capacity (q_e) rose from 12.18 to 14.38 mg g^{-1}, while the (R%) improved from 84.8% to 100% with rising temperature. This enhancement is attributed to the greater mobility of dye molecules at higher temperatures, which facilitates their transport from the bulk solution to the adsorbent surface. Higher temperature also promotes deeper penetration of dye molecules into the composite pores, thereby reducing diffusion resistance. In addition, thermal activation may improve the accessibility of active functional groups onto the surface of the adsorbent, enhancing the interaction with dye molecules.[75] The observed improvement in adsorption performance with temperature indicates that the process nature is endothermic. These findings also suggest that the Ca-alginate/PDA composite could be effectively applied in high-temperature wastewater treatment scenarios, where thermal energy can be harnessed to enhance dye removal efficiency.

3.3.7. Effect of ionic strength. The influence of ionic strength on BG dye adsorption by using the Ca-alginate/PDA composite was evaluated by using different NaCl concentrations from 0 to 0.5 mol L^{-1}, while the other conditions, such as contact time, initial concentration of dye, adsorbent dosage, pH, and temperature remain constant. As represented in Fig. S1 (in the SI), the (R%) rose significantly from 59.15% to 97.5% with increasing the concentration of NaCl, indicating a strong dependence of adsorption performance on the ionic strength of the medium. This enhancement can be explained by the salting-out effect, in which the solubility of dye molecules in water decreases with increasing salt concentration. Reduced solubility promotes aggregation of BG molecules through intermolecular forces such as van der Waals interactions and dipole–dipole attractions, which facilitates their uptake by the composite surface. Moreover, elevated ionic strength enhances dye molecule dimerization, further strengthening intermolecular associations and promoting adsorption onto the Ca-alginate/PDA composite.[76] These findings demonstrate that NaCl plays a dual role by both reducing dye solubility and intensifying molecular interactions, thereby enhancing adsorption efficiency. Such effects are particularly relevant for wastewater treatment processes, where high ionic strength is a common characteristic of industrial effluents.

3.4. Adsorption kinetics

The mechanism of adsorption and the rate-determining steps were investigated by different kinetic models, such as pseudo-second order (PSORE), Elvoich, pseudo-first order (PFORE), and

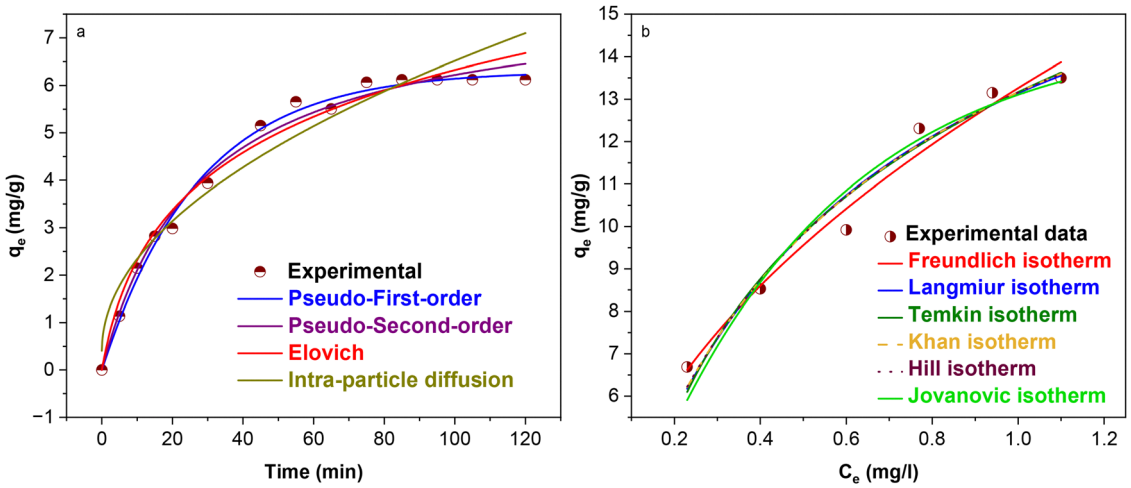

Fig. 4 Adsorption kinetic models of BG onto the Ca-alginate/PDA composite (a) and adsorption isotherms of BG onto the Ca-alginate/PDA composite (b).

intra-particle diffusion (IPD) models.[77–79] Fig. 4a illustrates the non-linear relation between q_t and time for this model. Table 1 also summarizes the corresponding correlation coefficients (R^2) and the kinetic model constants. The PFORE model indicates that the rate of adsorption depends on the availability of unoccupied sites on the surface of the adsorbent, while PSORE indicates that the process is controlled by a chemical adsorption mechanism, through the electron exchange between the adsorbate and the adsorbent. From Table 1, we found that the R^2 values of both PFORE and PSORE are very close to each other, suggesting that both kinetic processes can take place simultaneously at the surface of the polymer composite and both models can reasonably describe the adsorption kinetics within the investigated time range. Although the PFORE provides a slightly better statistical fit compared to the PSORE model, the q_e predicted by the PSORE (7.951 mg g^{-1}) is higher than that of the PFORE model (6.3068 mg g^{-1}) suggesting that while physical adsorption may dominate the early stages of the process, chemical interactions may also contribute to the overall adsorption behavior of BG dye on the Ca-alginate/PDA composite.[80] In addition, the rate limiting steps and the mechanism of BG dye adsorption onto the Ca-alginate/PDA composite, were studied using the IPD model. The IPD model indicates that different diffusion processes may be controlled by the adsorption process, such as film diffusion, bulk diffusion, and intra-particle diffusion. Fig. S2 (in the SI) presents that the adsorption capacity (q_t) displays a linear relationship with square root of time, confirming that intra-particle diffusion is a governing step in the system.[81] Moreover, the chemisorption kinetics of BG onto the Ca-alginate/PDA composite, were evaluated using the Elovich kinetic model, with the results summarized in Table 1. The high correlation coefficient (R^2 = 0.977) obtained from this model provides strong evidence that the adsorption of BG on the Ca-alginate/PDA composite proceeds through a chemisorption mechanism.

Table 1 Adsorption kinetics of BG dye onto Ca-alginate/PDA

Kinetic model	Mathematical equation	Kinetic constant	Calculated value
PFORE	$q_t = q_e(1 - e^{Kt})$	q_e (mg g^{-1})	6.306 ± 0.10
		K (min^{-1})	0.036 ± 0.001
		R^2	0.993
PSORE	$q_t = \frac{(q_e^2 k_2 t)}{(1 + q_e k_2 t)}$	q_e (mg g^{-1})	7.951 ± 0.25
		K_2 (g mg^{-1} min^{-1})	0.004 ± 0.004
		R^2	0.988
Elovich	$q_t = 1/\beta \ln(\alpha\beta t + 1)$	B (g mg^{-1})	0.488 ± 0.004
		α (mg g^{-1} min^{-1})	0.429 ± 0.007
		R^2	0.977
IPD	$q_t = K_{diff} t^{1/2} + C$	K_{diff} (mg g^{-1} $min^{-1/2}$)	0.61 ± 0.002
		C	0.406 ± 0.021
		R^2	0.978

3.5. Adsorption isotherms

Adsorption models are crucial for interpretation of the equilibrium interaction between the surface of the adsorbent and adsorbate molecules. Several isotherms' models were applied to fit the experimental data, such as the Langmuir, Dubinin–Radushkevich (D–R), Freundlich, Temkin, Jovanovic and Khan models. Fig. 4b illustrated their nonlinear fittings, with the calculated parameters listed in Table 2. According to the results in Table 2, we found that the R^2 value of both Langmuir and Freundlich models are close to each other, suggesting that both physisorption and chemosorption occur at the same time on the surface of the polymer composite. This behavior can be explained by considering that the adsorbate molecules first attach to the surface through weak physical interactions, allowing them to diffuse or align into favorable orientations. These initial interactions serve as a preparatory step that facilitates the subsequent formation of covalent or coordinative bonds during chemisorption. Such a sequential adsorption mechanism where physisorption precedes chemisorption is commonly observed in surface reaction processes.[82] The Ca-alginate/PDA composite exhibited a maximum adsorption capacity (q_m) of 19.817 mg g^{-1}, highlighting its strong efficiency

Table 2 Adsorption isotherm model of BG dye on Ca-alginate/PDA

Isotherm model	Mathematical equation	Isotherm constant	Value
Langmuir	$q_e = \frac{kq_{mC_e}}{1+kC_e}$	q_m (mg g^{-1})	19.817 ± 1.68
		K (L mg^{-1})	1.968 ± 0.40
		R^2	0.960
Freundlich	$q_e = k_F C_e^{1/n}$	K_F	13.25 ± 0.27
		n	2.11 ± 0.17
		R^2	0.973
Dubinin–Radushkevich	$q_e = q_m \exp^{-k\varepsilon^2}$	q_m (mol g^{-1})	0.001
	$\varepsilon = \left[RT \ln\left(1+\frac{1}{C_e}\right)\right]$	k (mol^2 J^{-2})	$3.33 \times 10^{-9} \pm 3 \times 10^{-10}$
	$E_a = \frac{1}{\sqrt{2k}}$	E_a (kJ mol^{-1})	12.253
		R^2	0.968
Temkin	$q_e = B \ln(kC_e)$	B	4.806 ± 0.002
		K (L mg^{-1})	15.470 ± 0.015
		R^2	0.999
Khan	$q_e = \frac{(q_{mkC_e})}{((1+kC_e)^n)}$	q_m (mg g^{-1})	17.136 ± 0.096
		k	2.351 ± 0.016
		n	0.924 ± 0.002
		R^2	0.999
Jovanovic	$q_e = q_m(1 - \exp^{-kC_e})$	q_m (mg g^{-1})	14.66 ± 0.015
		k	2.242 ± 0.005
		R^2	0.996

as an adsorbent. The D–R isotherm is used for microporous materials and is able to differentiate between physical adsorption and chemical adsorption processes through the value of free energy of adsorption (E_a). Its application to experimental data of BG dye adsorption onto the Ca-alginate/PDA composite (Fig. S3 in the SI), shows a good fitting (R^2 = 0.968). Also, the value of E_a was calculated to be 12.235 kJ mol^{-1}, this indicates that the BG dye adsorption onto the Ca-alginate/PDA composite is chemosorption. Similarly, the Temkin model, which assumes a linear decrease in the heat of adsorption with increasing coverage, demonstrated an excellent correlation (R^2 = 0.999), suggesting that the Ca-alginate/PDA composite surface has a uniform distribution of binding energies. Also, the obtained B value (4.806) reflects the variation of adsorption energy, while the relatively high k value (15.470) indicates strong binding affinity between the dye molecules and the active sites of the adsorbent. For the Khan model, the results also revealed a very good fit (R^2 = 0.999), further supporting its applicability. The parameter (n = 0.924), being close to unity, implies that the adsorbent surface is nearly homogeneous, where adsorption occurs without significant deviation from ideal monolayer behavior. Meanwhile, the value equal to 2.351 confirms a high affinity between the adsorbent and adsorbate. The Jovanovic model, modifies the Langmuir model to account for possible mechanical interactions of adsorbed and desorbed molecules, showed a slightly lower fit (R^2 = 0.996) compared to Langmuir. This indicates that while such interactions may occur, they have minimal influence on the overall adsorption mechanism.

3.6. Adsorption thermodynamics

Temperature is a crucial factor influencing a material's ability to eliminate BG dye from wastewater. The thermodynamic adsorption properties were studied at temperatures ranging from 298 K to 328 K. To understand the nature of adsorption of BG dye, several thermodynamic parameters, including Gibbs free energy (ΔG), enthalpy (ΔH), and entropy (ΔS), were evaluated. These parameters were calculated depending on the experimental data using Van's Hoff equations, as presented below:[83,84]

$$K = \frac{C_{AC}}{C_e} \quad (3)$$

$$\ln K = \frac{\Delta S}{R} - \frac{\Delta H}{RT} \quad (4)$$

$$\Delta G = \Delta H - T\Delta S \quad (5)$$

Here, R denotes the general constant of gas (8.314 J mol^{-1} K^{-1}), K is the thermodynamic equilibrium constant, T is the absolute temperature (K), C_e represents the concentration of BG dye in solution at equilibrium (mg L^{-1}), and CAC is the equilibrium quantity of BG dye adsorbed onto the composite (mg L^{-1}). A plot of $\ln K$ against $1/T$, shown in Fig. 5, was used to determine ΔS and ΔH from the intercept and the slope, respectively. The estimated values are listed in Table 3. The positive ΔH values at all temperatures indicate that the adsorption of BG is endothermic in nature. Furthermore, the positive ΔS values suggest an increase in disorder at the interface between the surface of the adsorbent and the dye molecules. Additionally, as the temperature rises, the adsorption becomes more spontaneous, and the ΔG value decreases, indicating that higher temperatures enhance the progression of the reaction.

3.7. Mechanism of adsorption

The BG dye adsorption on the prepared Ca-alginate/PDA composite occurs through several interaction mechanisms, namely π–π interactions, hydrogen bonding interaction, and electrostatic interactions as presented in Fig. 6. PDA units in the Ca-alginate/PDA composite have a π-conjugated aromatic structure

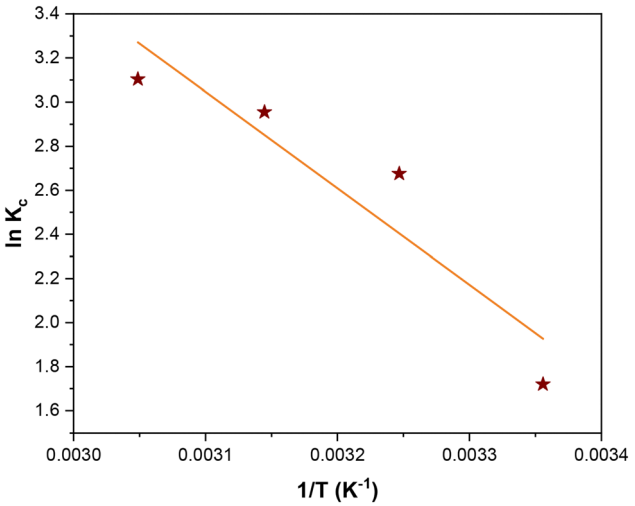

Fig. 5 Plot of ln K_c against $1/T$ for adsorption of BG dye onto Ca-alginate/PDA.

Table 3 Thermodynamic parameters of BG dye adsorption onto Ca-alginate/PDA

	Parameters		
Temperature (K)	ΔG (kJ mol^{-1})	ΔH (kJ mol^{-1})	ΔS (J mol^{-1} K^{-1})
298	−41.1358928	36.398692	138.162052
308	−42.51751332		
318	−43.89913384		
328	−45.28075436		

that enables stacking interactions with the aromatic rings of BG dye through π–π stacking interactions, enhancing dye affinity. Furthermore, hydroxyl (–OH) and carboxyl (–COOH) groups present in PDA or alginate can form hydrogen bonds with amine groups of BG dye molecules, thus enhancing the binding strength and stability of adsorption. In addition, electrostatic interaction can occur between the negative surface charge generated by the deprotonation of functional groups such as carboxylate (–COO$^-$) in alginate and cationic BG dye. This anion–cation attraction facilitates rapid and effective adsorption.

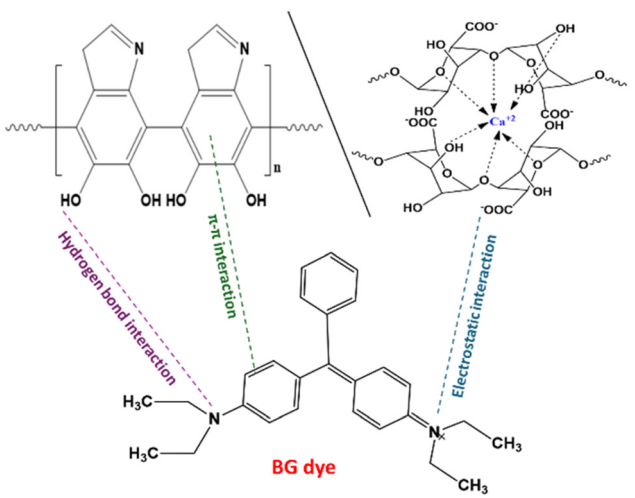

Fig. 6 Schematic presenting the interaction mechanisms between Ca-alginate/PDA and BG dye.

3.8. Recycling experiment

To illustrate the regeneration capability of the Ca-alginate/PDA composite as an adsorbent for removing BG dye from water, desorption experiments were carried out using a 0.5 mol L^{-1} HCl solution as the desorbing agent. The regeneration efficiency of the Ca-alginate/PDA composite after six cycles of adsorption–desorption processes is shown in Fig. 7a. The results indicated that there was no decrease in removal efficiency during the first four regeneration cycles, but a decline was observed in the sixth cycle. This reduction in removal efficiency may be due to the incomplete desorption of the BG dye absorbed on the Ca-alginate/PDA composite after repeated use. The findings suggest that the Ca-alginate/PDA composite can be effectively reused up to four times for BG removal from aqueous solutions. Additionally, these results confirm efficiency, reusability, stability, and high potential application of alginate for dye removal under the given experimental conditions. The FTIR spectra of Ca-alginate/PDA before and after regeneration are presented in Fig. 8b. The data indicate that the characteristic peaks corresponding to the functional groups of Ca-alginate/PDA remained unchanged even after six recycling cycles, indicating that the main chemical structure of the composite was preserved after multiple cycles. This confirms its efficiency, excellent reusability, structural stability, and strong potential for application in BG dye removal under the tested experimental conditions.

3.9. The checking of statistical analysis of data

3.9.1. Box–Behnken design. Box–Behnken design (BBD) was employed to evaluate the interactions between various variables. It was chosen in this study due to its simplicity, ability to minimize the number of required experiments, and effectiveness in providing accurate response predictions.[85,86] The experimental design contained 17 experiments with adsorption capacity (q_e) selected as the response surface variable. The outcomes of these experiments, including both the observed and predicted adsorption capacities, are shown in Table 4. The quadratic model used is described by eqn (6).

$$q_e = +2.94 + 0.4963 \times A - 1.31 \times B + 2.54 \times C - 0.9065 \times AB + 0.0592 \times AC - 1.31 \times BC \quad (6)$$

where A is the pH, B is the adsorbent dose and C is the BG dye concentration.

The reaction can be predicted at specific levels of each factor using the equation expressed in terms of coded variables (eqn (6)). Where the low and high levels of the factors are written as −1 and +1, respectively. By comparing the coefficients of these factors, the coded equation enables evaluation of the relative influence of each component.

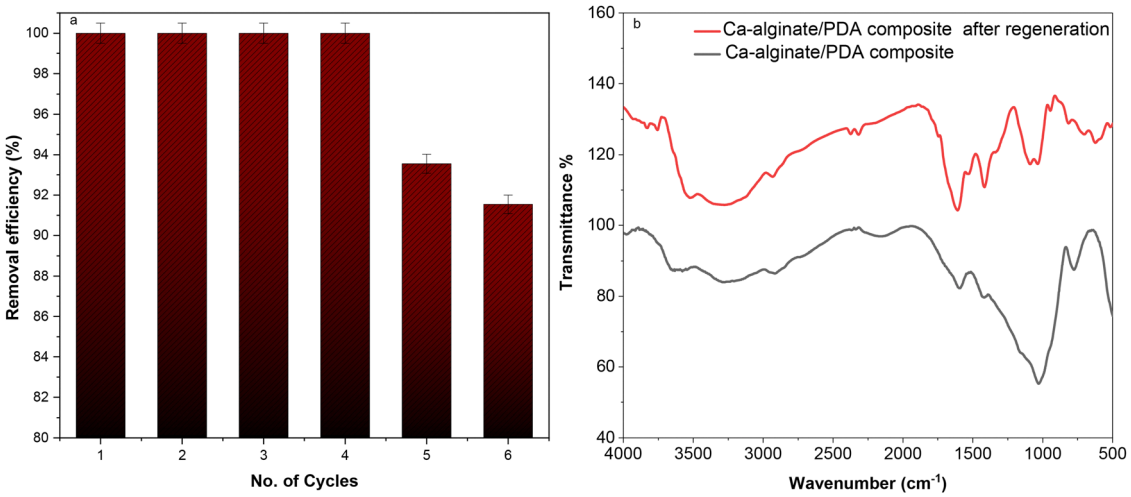

Fig. 7 (a) Regeneration efficiency of the Ca-alginate/PDA composite for BG dye adsorption; (b) FTIR spectra of the Ca-alginate/PDA composite before and after the regeneration process (b).

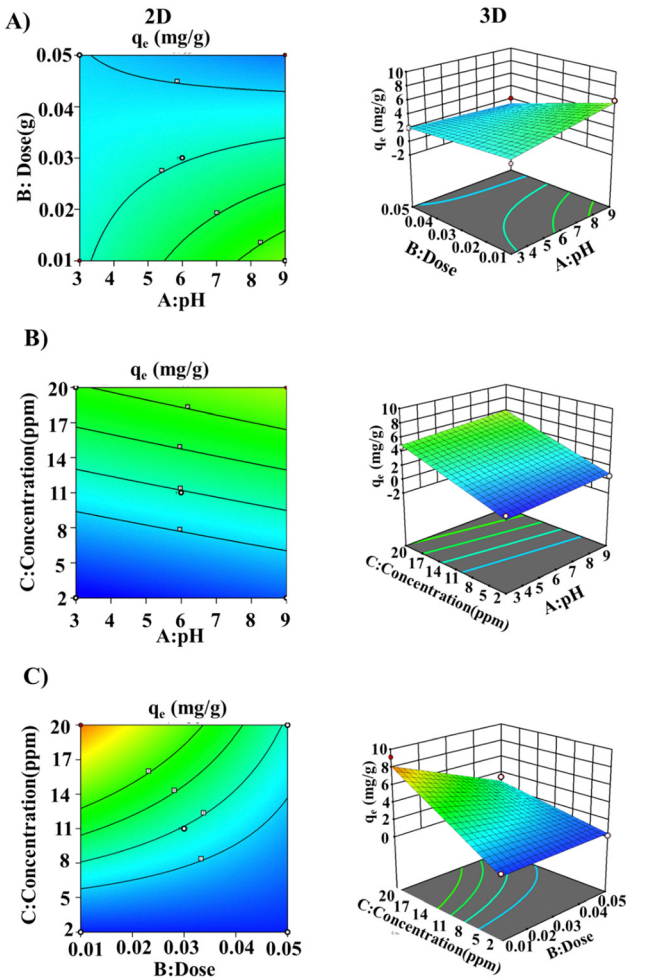

Fig. 8 The contour plots and 3D response surface represent the interaction between (a) dose and pH, (b) concentration and pH, and (c) concentration of dye and adsorbent dose for BG dye removal by using Ca-alginate/PDA.

Table 4 Results of adsorption capacity of Ca-alginate/PDA

	Factors			q_e (mg g^{-1})		
Run	pH	Dose (g)	Concentration (mg L^{-1})	Predicted	Experimental	Residual
1	3	0.05	11	2.04	2.02	−0.024
2	9	0.01	11	5.65	5.95	0.3
3	6	0.03	11	2.94	2.77	0.173
4	3	0.03	20	4.93	4.67	−0.260
5	6	0.03	11	2.94	2.77	−0.173
6	6	0.03	11	2.94	2.77	−0.173
7	6	0.01	20	8.10	9.12	1.02
8	3	0.03	2	−0.0304	0.466	0.505
9	6	0.03	11	2.94	2.77	−0.173
10	6	0.05	2	0.403	0.140	−0.263
11	9	0.03	20	6.04	4.93	−1.10
12	3	0.01	11	2.84	2.30	−0.544
13	6	0.05	20	2.86	3.37	0.501
14	6	0.01	2	0.393	0.650	0.256
15	6	0.03	11	2.94	2.77	−0.173
16	9	0.03	2	0.835	0.496	−0.339
17	9	0.03	11	1.22	2.04	0.820

Alternatively, the actual equation can be represented by eqn (7).

$$q_e = -4.1787 + 0.5945 \times \text{pH} + 105.841 \times \text{dose} + 0.4879 \times \text{concentration} - 15.10833 \times \text{pH} \times \text{dose} + 0.002191 \times \text{pH} \times \text{concentration} - 7.28750 \times \text{dose} \times \text{concentration} \quad (7)$$

For specifying values of each factor, the equation expressed in terms of the actual factors may be used to obtain the predictions regarding the reaction, with factor levels expressed in their original units. However, to assess the relative significance of each factor, this equation is not used, since the coefficients are scaled to measure units of each factor and the intercept does not correspond to at the point of the design space.

Table 5 Outcomes of ANOVA analysis for the response surface

Source	Sum of square	d*f*	Mean square	*F*-value	*P*-value	Remark	Standard error
Intercept							0.159
Model	77.51	6	12.92	30.03	<0.0001	Significant	
A (pH)	1.97	1	1.97	4.58	0.0580		0.231
B (dose)	13.66	1	13.66	31.75	0.0002		0.231
C (concentration)	51.69	1	51.69	120.18	<0.0001		0.231
AB	3.29	1	3.29	7.64	0.0200		0.327
AC	0.014	1	0.0140	0.032	0.860		0.327
BC	6.88	1	6.88	16.00	0.0025		0.327
Residual	4.30	10	0.4301				
Lack of fit	4.30	6	0.7169				
Pure error	0.000	4	0.0000				
Cor total	81.81	16					

ANOVA was conducted to examine the BG dye adsorption on the Ca-alginate/PDA composite, aiming to pinpoint the most influential factors and their interactions affecting the process, and to validate the model's reliability. ANOVA analysis also facilitates understanding the relationships between the process parameters and response variables *via* graphical data interpretation. The ANOVA analysis results of response surface experiments are summarized in Table 5. As shown in Table 5, the model is statistically significant, as evidenced by a high *F*-value (F = 30.03) and low *p*-value ($p < 0.05$), indicating that the selected variables collectively exert a meaningful influence on the adsorption process rather than arising from random variation. The probability that an *F*-value this great could occur due to noise is only 0.01 percent. Moreover, the coefficient of determination (R^2) measures how well the model accounts for variability in the response; an R^2 value close to 1 signifies a better model fit. As presented in Table 6, the coefficient of determination (R^2) was 0.947, and the adjusted R^2 was 0.915, both of which are close in value indicating that the model fits the data well. High values of R^2 and adjusted R^2 suggest strong accuracy and a strong correlation between experimental and predicted results. The predicted R^2 value of 0.737 also shows a good consistency with the value of adjusted R^2 of 0.915 as the difference between them is <0.2. While the model generally fits the experimental data well, some predicted values exhibited large residuals, particularly at the extremes of the experimental domain. These anomalies likely result from extrapolation beyond the region covered by the actual experiments. By focusing on the central domain of the design, the model provides reliable predictions and identifies optimal conditions. Adeq-precision, which reflects signal-to-noise ratio, is considered acceptable when it exceeds 4. The high Adeq-precision value (19.34) indicates a strong signal relative to noise, confirming that the model is sufficiently sensitive to detect the effects of the studied variables across the design space. This robustness supports the reliability of the model in identifying meaningful trends in the adsorption behavior. Additionally, a smaller standard deviation (0.655) value reflects a close agreement between experimental data and the model's predictions, suggesting that the model describes the adsorption response with good accuracy under the investigated conditions.

3.9.2. Response analysis for the capacity of adsorption. 3D plots of response surface along with their corresponding 2D contour plots provide valuable insights into how various parameters influence the response being studied. Using design-Expert software, a contour plot was generated to investigate the influences of various variable interactions on the adsorption of BG dye onto Ca-alginate/PDA. The interactions between pH, adsorbent dosage, and concentration of BG on the adsorption capacity were illustrated through both 2D and 3D plots. Fig. 8 presents the combined influence of these factors on BG adsorption. Firstly, in Fig. 8a, it is observed that increasing the pH initially enhances the adsorption capacity, but excessive adsorbent dosage leads to a decline in the adsorption capacity. Also, in Fig. 8b, the adsorption capacity rises with both increasing BG concentration and pH. Lastly, as shown in Fig. 8c, a higher initial BG concentration boosts the adsorption capacity, while increasing the adsorbent dose causes it to decline.

3.9.3. Adequacy checking of the BBD model. Clustering of data points around the straight line in Fig. 9a indicates a strong agreement between actual and predicted values, reflecting the model's high accuracy in forecasting adsorption capacity. Fig. 9b displays the relationship between externally studentized residuals and predicted values. The difference between predicted and observed values divided by their standard error can be represented by these standardized residuals and serves as an essential diagnostic tool in regression analysis. This relationship helps evaluate the model's overall fit, detect possible outliers, and understand residual trends. Fig. 9c and d illustrate how externally studentized residuals vary with the run

Table 6 Statistical summary of various models of adsorption of BG dye on Ca-alginate/PDA

Source	Std. Dev.	*p*-value	PRESS	R^2	Adjusted R^2	Predicted R^2	Remark
Linear	1.06	< 0.0001	30.17	0.822	0.782	0.631	
2FI	**0.655**	**0.0054**	**21.49**	**0.947**	**0.915**	**0.733**	**Suggested**
Quadratic	0.669	0.5033	50.23	0.912	0.912	0.386	
Cubic	1.49×10^{-6}	< 0.0001		1.000	1.000		**Aliased**

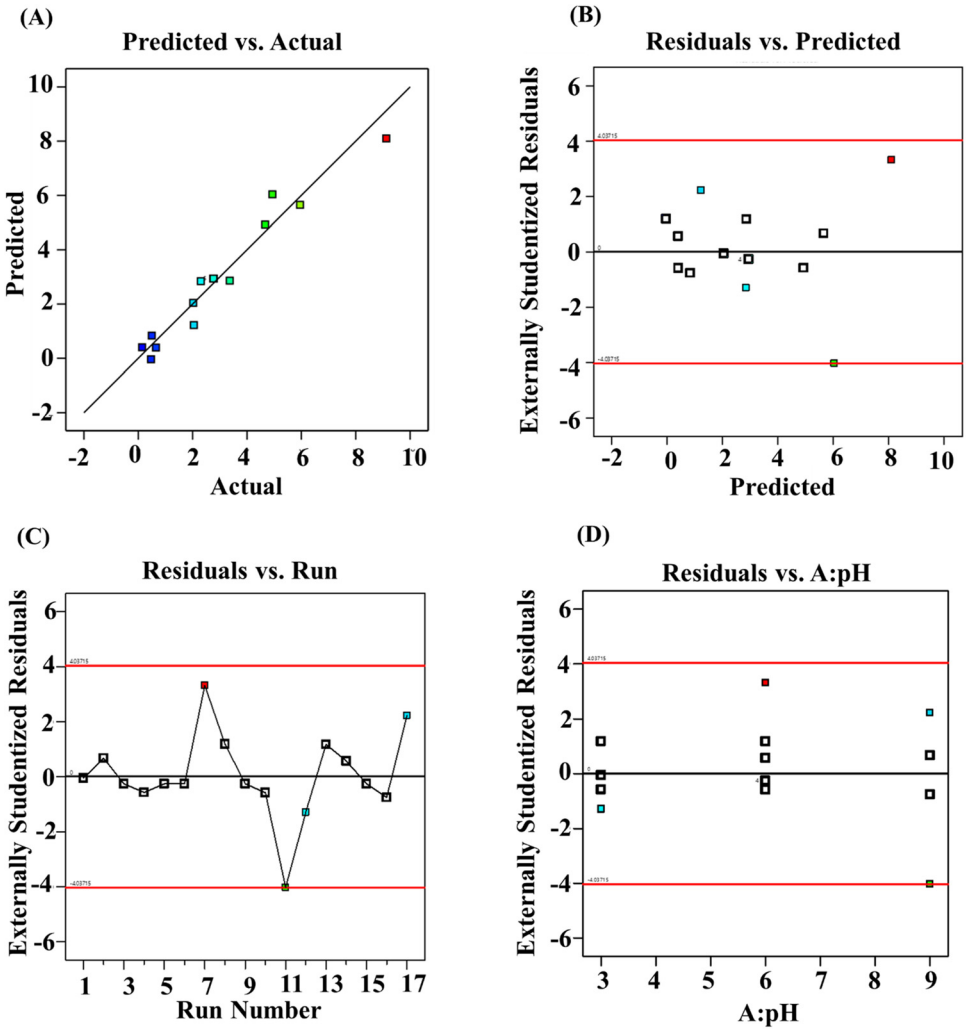

Fig. 9 (a)–(d) Experimental capacity of adsorption compared to predicted capacity of adsorption.

number, offering insight into changes in residuals throughout the experimental sequence. This allows for the identification of any recurring patterns or irregularities associated with the experiment order. By plotting residuals against run numbers, any trends tied to specific runs can be detected, potentially indicating systematic issues in experimental execution, data collection, or measurement consistency. Identifying such trends is key to maintaining the accuracy and reliability of the experimental outcomes.

3.10. Comparison with other adsorbents reported in the literature

To evaluate the effectiveness of the Ca-alginate/PDA composite in removing BG dye, its removal efficiency was compared with

Table 7 Comparison of the removal efficiency of the Ca-alginate/PDA composite with other adsorbents for BG dye removal

		Reaction conditions				
No.	Adsorbent	Dye conc. (mg L^{-1})	Dose (g)	Time (min)	Removal (%)	Ref.
1	Ca-alginate/PDA	7	0.1	75	99.07	Present study
2	Poly(DVB)	7.5	0.05	120	97.4	32
3	Poly(AN-*co*-AMPS)	7.5	0.1	80	99.5	31
4	Hydroxyapatite/chitosan	5	0.9	90	80	87
5	Magnetic RHA	5	0.5	60	79.4	88
6	Polyacrylonitrile/silver nanocomposite	45.45	0.03	120	90	9
7	ZnO/PPy nanocomposite	90	0.075	90	90.2	52
8	(CNSAC)	50	0.1	90	99	15
9	Ni–Gd$(OH)_3$	10	0.01	300	90	89
10	Kaolin	20	1	90	91	63

other reported adsorbents, as presented in Table 7. While direct comparisons are challenging due to differences in experimental conditions, such as dye concentration, adsorbent dosage, and contact time, Ca-alginate/PDA stands out as one of the most efficient materials. It demonstrates excellent removal efficiency, achieving 99% efficiency under relatively mild conditions (initial dye concentration of 7 mg L^{-1}, adsorbent dosage of 0.1 g, and time of 75 minutes). Additionally, the Ca-alginate/PDA composite has the ability to maintain stability over six consecutive regeneration cycles, as shown in the desorption studies, highlighting its promise as a sustainable and cost-effective material for use in large-scale water purification.

4. Conclusions

This work successfully demonstrated excellent adsorption performance, cost efficiency, and sustainability of Ca-alginate/PDA for the removal of toxic BG dye from wastewater. The prepared biopolymer has distinctive features; for example, its large surface area and porous structure greatly contributed to its enhanced adsorption capability. Also, it provided extra benefits, such as low-cost recyclability, environmental friendliness, and stability. Functional groups present in the Ca-alginate/PDA facilitated strong interactions with the molecules of dye *via* different interaction mechanisms like electrostatic attraction, π–π stacking, and hydrogen bonding, achieving a maximum removal efficiency of 99.07% under optimal conditions. Specifically, PDA provided aromatic rings and hydroxyl groups that promoted π–π interactions and hydrogen bonding with dye molecules, while Ca-alginate contributed a carboxylate-rich, negatively charged network responsible for electrostatic attraction with cationic BG dye. Kinetic analysis indicated that the adsorption followed a pseudo-first-order model, while isotherm data aligned best with the Freundlich model, suggesting multilayer adsorption on a heterogeneous surface. Thermodynamic results confirmed that the process was both endothermic and spontaneous, with higher temperatures further promoting dye uptake, highlighting its practical applicability. The study also utilized (BBD) to systematically assess the impact of key operational factors on adsorption efficiency. Response surface methodology (RSM) offered detailed insights into variable interactions, leading to adsorption process optimization. Furthermore, Ca-alginate/PDA demonstrated effective regeneration using hydrochloric acid and retained reasonable adsorption performance over four reuse cycles, making it an eco-friendlier and more cost-efficient alternative to traditional adsorbents. While these results are promising, long-term structural stability and resistance to fouling in real wastewater matrices require further investigation. Overall, Ca-alginate/PDA shows promising adsorption efficiency and thermal stability, suggesting its suitability as an adsorbent for dye removal, providing an effective and sustainable approach to combat dye contamination in aquatic systems.

Author contributions

Marwa Magd: experiments, analysis, investigation, resources, and writing – original draft; Mohamed Aboelnga: project administration, conceptualization, methodology, calculation, investigation, and writing – review and editing; Elsayed Elbayoumy: project administration, conceptualization, validation, formal analysis, investigation, resources, data curation, and writing – review and editing.

Conflicts of interest

The authors declare that they have no known competing financial interests or personal relationships that could have appeared to influence the work reported in this paper.

Data availability

The data that support the findings of this study are available from the corresponding author upon reasonable request.

Supplementary information (SI) is available. See DOI: https://doi.org/10.1039/d5ma01333j.

Acknowledgements

This research did not receive any specific grant from funding agencies in the public, commercial, or not-for-profit sectors.

References

1 E. Elbayoumy, M. O. Elassi, G. M. Khairy, E. A. Moawed and M. M. aboelnga, Development of efficient fluorescent sensor for the detection of hazard aromatic nitro compounds *via* *N*-(1-naphthyl)ethylenediamine: Experimental and DFT studies, *J. Mol. Liq.*, 2023, **391**, 123270. Available from: https://www.sciencedirect.com/science/article/pii/S0167732223020767.

2 K. Sukla and U. Kumar, South African Journal of Chemical Engineering Adsorption of brilliant green dye from aqueous solution onto chemically modified areca nut husk, *S. Afr. J. Chem. Eng.*, 2021, **35**, 33–43, DOI: 10.1016/j.sajce.2020.11.001.

3 E. Elbayoumy, M. Shaker, M. Gaafar, E. A. Moawed and M. M. Aboelnga, Eco-friendly one-step production of a highly sensitive fluorescent sensor for iron (III) detection in aqueous solutions: Experimental and DFT insights, *J. Photochem. Photobiol., A*, 2025, **466**, 116391.

4 E. Elbayoumy, M. Elhendawy, M. M. Gaafar, E. Moawed and M. M. aboelnga, Novel fluorescent sensor based on triazole-pyridine derivative for selective detection of mercury (II) ions in different real water samples: Experimental and DFT calculations, *J. Mol. Liq.*, 2024, **401**, 124589.

5 M. Berradi, R. Hsissou, M. Khudhair, M. Assouag, O. Cherkaoui and A. El Bachiri, *et al.*, Textile finishing dyes and their impact on aquatic environs, *Heliyon.*, 2019, **5**(11), e02711.

6 P. Parthipan, L. Cheng, A. Rajasekar, M. Govarthanan and A. Subramania, Biologically reduced graphene oxide as a

green and easily available photocatalyst for degradation of organic dyes, *Environ. Res.*, 2021, **196**, 110983.

7 M. T. Mosisa, P. Zhang, B. Wu, L. Chen, Z. Su and P. Li, *et al.*, Synthesis and characterization of Ce-BiOBr/Bi2S3 catalyst with enhanced catalytic activity for organic dye reduction under dark, *J. Environ. Chem. Eng.*, 2024, **12**(5), 113383. Available from: https://www.sciencedirect.com/science/article/pii/S2213343724015136.

8 M. K. Dahri, L. B. L. Lim, M. R. R. Kooh and C. M. Chan, Adsorption of brilliant green from aqueous solution by unmodified and chemically modified Tarap (Artocarpus odoratissimus) peel, *Int. J. Environ. Sci. Technol.*, 2017, **14**(12), 2683–2694.

9 O. Abd Al-Qader Mahmood and B. I. Waisi, Synthesis and characterization of polyacrylonitrile based precursor beads for the removal of the dye malachite green from its aqueous solutions, *Desalin. Water Treat.*, 2021, **216**, 445–455.

10 T. A. Aragaw, A review of dye biodegradation in textile wastewater, challenges due to wastewater characteristics, and the potential of alkaliphiles, *J. Hazard. Mater. Adv.*, 2024, **16**, 100493.

11 B. Saha, G. Shil, A. Debnath and B. Saha, Process optimization of victoria blue dye removal using polypyrrole-encapsulated zirconium oxide: Mechanistic pathway and economic assessment, *J. Indian Chem. Soc.*, 2024, **101**(11), 101407.

12 V. L. Gole and P. R. Gogate, Degradation of brilliant green dye using combined treatment strategies based on different irradiations, *Sep. Purif. Technol.*, 2014, **133**, 212–220.

13 R. Mansour, M. G. Simeda and A. Zaatout, Adsorption studies on brilliant green dye in aqueous solutions using activated carbon derived from guava seeds by chemical activation with phosphoric acid, *Desalin. Water Treat.*, 2020, **202**, 396–409.

14 M. Abbas, Removal of brilliant green (BG) by activated carbon derived from medlar nucleus (ACMN) – Kinetic, isotherms and thermodynamic aspects of adsorption, *Adsorpt. Sci. Technol.*, 2020, **38**(9–10), 464–482.

15 P. Samiyammal, A. Kokila, L. A. Pragasan, R. Rajagopal, R. Sathya and S. Ragupathy, *et al.*, Adsorption of brilliant green dye onto activated carbon prepared from cashew nut shell by KOH activation: Studies on equilibrium isotherm, *Environ. Res.*, 2022, **212**(PD), 113497, DOI: 10.1016/j.envres.2022.113497.

16 M. Farhan Hanafi and N. Sapawe, A review on the water problem associate with organic pollutants derived from phenol, methyl orange, and remazol brilliant blue dyes, *Mater. Today: Proc.*, 2020, **31**, A141–A150.

17 G. Arunkumar, G. Deviga, M. Mariappan, M. Pannipara, A. G. Al-Sehemi and U. A. Soliman, *et al.*, Carbon encapsulated ZnO nanoplates for efficient removal of organic dyes from aqueous medium by adsorption: Role of organic ligand and calcination temperature, *J. Mol. Liq.*, 2024, **403**, 124852. Available from: https://www.sciencedirect.com/science/article/pii/S0167732224009085.

18 X. Yan, M. Chen, J. Wang, Z. Wang, R. Xin and D. Wu, *et al.*, Nanoarchitectonics of bamboo-based heterojunction photocatalyst for effective removal of organic pollutants, *Chem. Eng. J.*, 2024, **495**, 153431. Available from: https://www.sciencedirect.com/science/article/pii/S1385894724049209.

19 A. B. Bassa, O. A. Zelekew, T. A. Meresa and T. A. Berhe, Croton macrostachyus leaf-mediated biosynthesis of copper oxide nanoparticles for enhanced catalytic reduction of organic dyes, *Mater. Res. Express*, 2024, **11**(8), 085001.

20 S. Satyam and S. Patra, Innovations and challenges in adsorption-based wastewater remediation: A comprehensive review, *Heliyon.*, 2024, **10**(9), e29573.

21 A. Kassa, A. Engida and M. Endaye, Eco-friendly adsorbents for industrial dye removal: A comprehensive review of low-cost alternatives, *Desalin. Water Treat.*, 2025, **323**, 101362.

22 M. A. Dominguez, M. Etcheverry and G. P. Zanini, Evaluation of the adsorption kinetics of brilliant green dye onto a montmorillonite/alginate composite beads by the shrinking core model, *Adsorption*, 2019, **25**(7), 1387–1396, DOI: 10.1007/s10450-019-00101-w.

23 S. Das, S. R. Paul and A. Debnath, Enhanced performance of Lagerstroemia speciosa seed biochar and polypyrrole composite for the sequestration of emerging contaminant from wastewater sample: Case study of ofloxacin drug, *J. Water Process Eng.*, 2024, **64**, 105699.

24 D. Robati, B. Mirza, M. Rajabi, O. Moradi, I. Tyagi and S. Agarwal, *et al.*, Removal of hazardous dyes-BR 12 and methyl orange using graphene oxide as an adsorbent from aqueous phase, *Chem. Eng. J.*, 2016, **284**, 687–697, DOI: 10.1016/j.cej.2015.08.131.

25 M. M. Altayan, N. Tzoupanos and M. Barjenbruch, Polymer based on beta-cyclodextrin for the removal of bisphenol A, methylene blue and lead(II): Preparation, characterization, and investigation of adsorption capacity, *J. Mol. Liq.*, 2023, **390**, 122822.

26 S. Pandey, N. Son and M. Kang, Synergistic sorption performance of karaya gum crosslink poly(acrylamide-*co*-acrylonitrile) @ metal nanoparticle for organic pollutants, *Int. J. Biol. Macromol.*, 2022, **210**, 300–314.

27 M. R. El-Aassar, O. M. Ibrahim, B. M. Omar, H. T. A. El-Hamid, I. H. Alsohaim and H. M. A. Hassan, *et al.*, Hybrid Beads of Poly(Acrylonitrile-*co*-Styrene/Pyrrole)@Poly Vinyl Pyrrolidone for Removing Carcinogenic Methylene Blue Dye Water Pollutant, *J. Polym. Environ.*, 2023, **31**(7), 2912–2929.

28 M. Ajmal, S. Demirci, M. Siddiq, N. Aktas and N. Sahiner, Amidoximated poly(acrylonitrile) particles for environmental applications: Removal of heavy metal ions, dyes, and herbicides from water with different sources, *J. Appl. Polym. Sci.*, 2016, **133**(7), 1–11.

29 E. Elbayoumy, A. A. El-Bindary, T. Nakano and M. M. Aboelnga, Silver nanoparticles immobilized on crosslinked vinyl polymer for catalytic reduction of nitrophenol: experimental and computational studies, *Sci. Rep.*, 2025, **15**(1), 717.

30 E. Elbayoumy, E. M. Ibrahim, A. El-Bindary, T. Nakano and M. M. Aboelnga, Revealing an efficient copper oxide

nanoparticle catalyst for the reduction of the hazardous nitrophenol: experimental and DFT studies, *Mater. Adv.*, 2025, 6291–6304.

31 Y. A. Aggour, E. R. Kenawy, M. Magdy and E. Elbayoumy, Multifunctional copolymers for brilliant green dye removal: adsorption kinetics, isotherm and process optimization, *Environ. Sci.: Adv.*, 2025, **4**(5), 787–808.

32 M. Magdy, M. M. Aboelnga, A. Deyab, A. Semida, R. Rizk and N. Elseady, *et al.*, Experimental and theoretical investigations of divinylbenzene-based polymer as an efficient adsorbent for brilliant green dye removal, *RSC Adv.*, 2025, **15**(25), 19843–19858.

33 D. Tao, C. Tian, Y. Zhou, L. Pei and F. Zhang, Effective removal of brilliant green with magnetic barium phosphate composites: factor analysis and mechanism study, *Environ. Sci. Pollut. Res.*, 2023, **30**(17), 50364–50375.

34 M. El-Ghobashy, H. Hashim, M. Darwish, M. Khandaker, A. Sulieman and N. Tamam, *et al.*, Eco-Friendly NiO/Polydopamine Nanocomposite for Efficient Removal of Dyes from Wastewater, *Nanomaterials*, 2022, **12**(7), 1103.

35 A. S. Ben, L. Aloui, L. Mansour and F. Ayari, Synthesized and characterization of calcium alginate beads as biosorbent of pollutants dye and phosphate from aqueous solution, *Desalin. Water Treat.*, 2023, **314**, 199–209.

36 K. Sriphumrat, Y. Wongnongwa, S. Jungsuttiwong, P. Pakawanit, W. Sajomsang and J. B. Bremner, *et al.*, Physicochemical investigation of the enhanced removal of methylene blue from aqueous solution using polydopamine/silver nanoparticles, *J. Text. Inst.*, 2023, **114**(4), 562–573.

37 A. M. Aljeboree and A. F. Alkaim, Studying removal of anionic dye by prepared highly adsorbent surface hydrogel nanocomposite as an applicable for aqueous solution, *Sci. Rep.*, 2024, **14**(1), 9102.

38 P. Kumari, D. Kaushal, V. Chauhan, P. Shandilya and M. Kumar, Synthesis of gum acacia-cl-acrylic acid-*co*-itaconic acid hydrogels for efficient removal of toxic dye rhodamine-B: A step for sustainable environment, *Int. J. Biol. Macromol.*, 2025, **292**, 139296.

39 A. M. Aljeboree, A. F. Alkaim, S. A. Hussein, M. Abed Jawad, I. Hasan and S. A. Khuder, Synthesis and swelling behavior of highly adsorbent hydrogel for the removal of brilliant green from an aqueous solution: Thermodynamic, kinetic, and isotherm models, *Case Stud. Chem. Environ. Eng.*, 2024, **10**, 100831.

40 G. Ohemeng-Boahen, D. D. Sewu, H. N. Tran and S. H. Woo, Enhanced adsorption of congo red from aqueous solution using chitosan/hematite nanocomposite hydrogel capsule fabricated via anionic surfactant gelation, *Colloids Surf., A*, 2021, **625**, 126911.

41 A. M. Aljeboree, I. T. Hasan, A. Al-Warthan and A. F. Alkaim, Preperation of sodium alginate-based SA-g-poly(ITA-*co*-VBS)/RC hydrogel nanocomposites: And their application towards dye adsorption, *Arabian J. Chem.*, 2024, **17**(3), 105589.

42 H. Mittal, A. Maity and S. S. Ray, Gum ghatti and poly (acrylamide-*co*-acrylic acid) based biodegradable hydrogel-evaluation of the flocculation and adsorption properties, *Polym. Degrad. Stab.*, 2015, **120**, 42–52.

43 A. M. Aljeboree, A. F. Alkaim, F. H. Alsultany and S. K. Issa, Highly Reusable Nano Adsorbent Based on Clay-Incorporated Hydrogel Nanocomposite for Cationic Dye Adsorption, *J. Inorg. Organomet. Polym. Mater.*, 2025, **35**(2), 1165–1186.

44 A. M. Aljeboree, S. A. Hussein, U. S. Altimari, S. M. Mohealdeen, F. H. Alsultany and A. F. Alkaim, Optimization of swelling and mechanical behavior of novel pH-sensitive terpolymer biocomposite hydrogel based on activated carbon for removal brilliant blue dye from aqueous solution, *Polym. Bull.*, 2025, **82**(5), 1447–1478.

45 V. U. Siddiqui, R. A. Ilyas, S. M. Sapuan, N. H. A. Hamid, P. S. Khoo and A. Chowdhury, *et al.*, Alginate-based materials as adsorbent for sustainable water treatment, *Int. J. Biol. Macromol.*, 2025, **298**, 139946.

46 R. Chen, B. Lin and R. Luo, Recent progress in polydopamine-based composites for the adsorption and degradation of industrial wastewater treatment, *Heliyon.*, 2022, **8**(12), e12105.

47 M. T. ALSamman and J. Sánchez, Chitosan- and Alginate-Based Hydrogels for the Adsorption of Anionic and Cationic Dyes from Water, *Polymers*, 2022, **14**(8), 1498.

48 Y. Liu, Y. Sui, C. Liu, C. Liu, M. Wu and B. Li, *et al.*, A physically crosslinked polydopamine/nanocellulose hydrogel as potential versatile vehicles for drug delivery and wound healing, *Carbohydr. Polym.*, 2018, **188**, 27–36.

49 G. A. A. M. Al-Hazmi, A. A. Alayyafi, M. G. El-Desouky and A. A. El-Bindary, Guava seed activated carbon loaded calcium alginate aerogel for the adsorption of diclofenac sodium: Characterization, isotherm, kinetics, and optimization via Box-Behnken design, *Int. J. Biol. Macromol.*, 2024, **262**, 129995.

50 N. N. Bahrudin, Evaluation of degradation kinetic and photostability of immobilized TiO2/activated carbon bilayer photocatalyst for phenol removal, *Appl. Surf. Sci. Adv.*, 2022, **7**, 100208.

51 H. Abdel-Shafy, M. Hefny, H. M. Ahmed and F. Abdel-Haleem, Removal of Cadmium, Nickel, and Zinc from aqueous solutions by activated carbon prepared from corncob - waste agricultural materials, *Egypt. J. Chem.*, 2021, **0**(0), 0–0.

52 M. Zhang, L. Chang, Y. Zhao and Z. Yu, Fabrication of Zinc Oxide/Polypyrrole Nanocomposites for Brilliant Green Removal from Aqueous Phase, *Arabian J. Sci. Eng.*, 2019, **44**(1), 111–121.

53 H. Li and J. Qu, Mussel-inspired synthesis of silver nanoparticles as fillers for preparing waterborne polyurethane/Ag nanocomposites with excellent mechanical and antibacterial properties, *Polym. Int.*, 2022, **71**(1), 146–153.

54 M. Faried, M. Miyake, Z. Zakaria, M. Faried, K. Shameli and M. Miyake, *et al.*, Ultrasound-Assisted in the Synthesis of Silver Nanoparticles Using Sodium Alginate Mediated by Green Method, *Dig. J. Nanomater. Bios.*, 2016, **11**, 547–552.

55 M. Kuczajowska-Zadrożna, U. Filipkowska and T. Jóźwiak, Adsorption of Cu (II) and Cd (II) from aqueous solutions by

chitosan immobilized in alginate beads, *J. Environ. Chem. Eng.*, 2020, **8**(4), 103878.
56 H. Hemmatpour, O. De Luca, D. Crestani, M. C. A. Stuart, A. Lasorsa and P. C. A. van der Wel, *et al.*, New insights in polydopamine formation via surface adsorption, *Nat. Commun.*, 2023, **14**(1), 664.
57 Y. Xu, J. Sun, L. Qian and J. Li, Effect of gas-condensed phase synergistic system of 9,10-dihydro-9-oxo-10-phosphaphenanthrene-10-oxide and polydopamine on flame retardancy of epoxy resin, *J. Appl. Polym. Sci.*, 2021, **138**(3), 49698.
58 S. Rella, E. Mazzotta, A. Caroli, M. De Luca, C. Bucci and C. Malitesta, Investigation of polydopamine coatings by X-ray Photoelectron Spectroscopy as an effective tool for improving biomolecule conjugation, *Appl. Surf. Sci.*, 2018, **447**, 31–39.
59 W. Rajapaksha, I. H. W. Nicholas, T. Thoradeniya, D. N. Karunaratne and V. Karunaratne, Novel alginate nanoparticles for the simultaneous delivery of iron and folate: a potential nano-drug delivery system for anaemic patients, *RSC Pharm.*, 2024, **1**(2), 259–271.
60 F. Wang, R. Han, G. Liu, H. Chen, T. Ren and H. Yang, *et al.*, Construction of polydopamine/silver nanoparticles multilayer film for hydrogen peroxide detection, *J. Electroanal. Chem.*, 2013, **706**, 102–107.
61 B. D. Zdravkov, J. J. Čermák, M. Šefara and J. Janků, Pore classification in the characterization of porous materials: A perspective, *Cent. Eur. J. Chem.*, 2007, **5**(2), 385–395.
62 Y. A. Aggour, E. R. Kenawy, M. Magdy and E. Elbayoumy, Establishing a productive heterogeneous catalyst based on silver nanoparticles supported on a crosslinked vinyl polymer for the reduction of nitrophenol, *RSC Adv.*, 2024, **14**(41), 30127–30139.
63 B. K. Nandi, A. Goswami and M. K. Purkait, Adsorption characteristics of brilliant green dye on kaolin, *J. Hazard. Mater.*, 2009, **161**(1), 387–395.
64 S. Senapati, J. Giri, L. Mallick, D. Singha, T. K. Bastia and P. Rath, *et al.*, Rapid adsorption of industrial cationic dye pollutant using base-activated rice straw biochar: performance, isotherm, kinetic and thermodynamic evaluation, *Discov. Sustain.*, 2025, **6**(1), 46.
65 S. Guo, Z. Zou, Y. Chen, X. Long, M. Liu and X. Li, *et al.*, Synergistic effect of hydrogen bonding and π–π interaction for enhanced adsorption of rhodamine B from water using corn straw biochar, *Environ. Pollut.*, 2023, **320**, 121060.
66 H. N. Tran, S. J. You and H. P. Chao, Insight into adsorption mechanism of cationic dye onto agricultural residues-derived hydrochars: Negligible role of π–π interaction, *Korean J. Chem. Eng.*, 2017, **34**(6), 1708–1720.
67 N. F. Al-Harby, E. F. Albahly and N. A. Mohamed, Kinetics, Isotherm and Thermodynamic Studies for Efficient Adsorption of Congo Red Dye from Aqueous Solution onto Novel Cyanoguanidine-Modified Chitosan Adsorbent, *Polymers*, 2021, **13**, 4446.
68 M. Ali Khan, R. Govindasamy, A. Ahmad, M. R. Siddiqui, S. A. Alshareef and A. A. Hakami, *et al.*, Carbon Based Polymeric Nanocomposites for Dye Adsorption: Synthesis, Characterization, and Application, *Polymers*, 2021, **13**, 419.
69 J. Hou, Y. Zhou, J. Shan, C. Gu, T. Zhang and B. Wu, Quinoline and cholesterol based organogelator for selective adsorption of cationic dyes, *Colloids Surf., A*, 2024, **700**, 134851, DOI: 10.1016/j.colsurfa.2024.134851.
70 M. T. Yagub, T. K. Sen, S. Afroze and H. M. Ang, Dye and its removal from aqueous solution by adsorption: A review, *Adv. Colloid Interface Sci.*, 2014, **209**, 172–184. Available from: https://www.sciencedirect.com/science/article/pii/S0001868614001389.
71 R. J. Khan, A. N. S. Saqib, R. Farooq, R. Khan and M. Siddique, Removal of Congo Red from Aqueous Solutions by Spent Black Tea as Adsorbent, *J. Water Chem. Technol.*, 2018, **40**(4), 206–212.
72 E. Rápó and S. Tonk, Factors Affecting Synthetic Dye Adsorption; Desorption Studies: A Review of Results from the Last Five Years (2017–2021), *Molecules*, 2021, **26**(17), 5419.
73 B. K. Nandi and S. Patel, Effects of operational parameters on the removal of brilliant green dye from aqueous solutions by electrocoagulation, *Arabian J. Chem.*, 2017, **10**, S2961–S2968, DOI: 10.1016/j.arabjc.2013.11.032.
74 E. J. E. Abdelrazek, A. A. Gahlan, G. A. Gouda and A. S. A. Ahmed, Cost-effective adsorption of cationic dyes using ZnO nanorods supported by orange peel-derived carbon, *Sci. Rep.*, 2025, **15**(1), 4123.
75 H. Kamarden, M. Abu Hassan MohdA, Z. Z. Noor, R. R. Ibrahim and A. M. Evuti, Effect of Temperature and Air flow rate on Xylene Removal from Wastewater using Packed Column Air Stripper, *J. Teknol. Lab.*, 2014, **67**(4), 41–44.
76 S. Sadeghy, S. M. Pormazar, M. T. Ghaneian, M. H. Ehrampoush and A. Dalvand, Modeling and optimization of direct dyes removal from aqueous solutions using activated carbon produced from sesame shell waste, *Sci. Rep.*, 2024, **14**(1), 24867.
77 A. I. Adeogun, M. A. Idowu, A. E. Ofudje, S. O. Kareem and S. A. Ahmed, Comparative biosorption of Mn(II) and Pb(II) ions on raw and oxalic acid modified maize husk: Kinetic, thermodynamic and isothermal studies, *Appl. Water Sci.*, 2013, **3**(1), 167–179.
78 M. Musah, Y. Azeh, J. Mathew, M. Umar, Z. Abdulhamid and A. Muhammad, Adsorption Kinetics and Isotherm Models: A Review, *Caliphate J. Sci. Technol.*, 2022, **4**(1), 20–26.
79 J. Wang and X. Guo, Adsorption kinetic models: Physical meanings, applications, and solving methods, *J. Hazard. Mater.*, 2020, **390**, 122156.
80 N. Eldomiaty, E. Elbayoumy, M. M. Aboelnga and M. R. Mostafa, Repurposing waste plastic into a sustainable adsorbent for removing synthetic dye: experimental, optimization and theoretical modeling, *RSC Adv.*, 2026, **16**(2), 1008–1029.
81 S. P. Dharmarathna and N. Priyantha, Investigation of boundary layer effect of intra-particle diffusion on methylene blue adsorption on activated carbon, *Energy Nexus*, 2024, **14**, 100294.
82 N. E. Richey, C. de Paula and S. F. Bent, Understanding chemical and physical mechanisms in atomic layer deposition, *J. Chem. Phys.*, 2020, **152**(4), 040902.

83 K. Y. Foo and B. H. Hameed, An overview of dye removal via activated carbon adsorption process, *Desalin. Water Treat.*, 2010, **19**(1–3), 255–274.
84 S. Kanwal, P. Devi, Z. Ahmed and N. A. Qambrani, Adsorption isotherm, kinetic and thermodynamic studies for adsorption of fluoride on waste marble powder, *Desalin. Water Treat.*, 2024, **319**, 100441.
85 S. M. Haque, H. Rahman, N. Rahman, S. N. H. Azmi, O. Ashwaq and S. M. Wabaidur, *et al.*, Application of Box–Behnken design combined response surface methodology to optimize HPLC and spectrophotometric techniques for quantifying febuxostat in pharmaceutical formulations and spiked wastewater samples, *Microchem. J.*, 2023, **184**, 108191.
86 M. G. El-Desouky, A. A. A. Alayyafi, G. A. A. M. Al-Hazmi and A. A. El-Bindary, Effect of metal organic framework alginate aerogel composite sponge on adsorption of tartrazine from aqueous solutions: Adsorption models, thermodynamics and optimization via Box-Behnken design, *J. Mol. Liq.*, 2024, **399**, 124392, DOI: 10.1016/j.molliq.2024.124392.
87 A. Ragab, I. Ahmed and D. Bader, The removal of Brilliant Green dye from aqueous solution using nano hydroxyapatite/chitosan composite as a sorbent, *Molecules*, 2019, **24**(5), 847.
88 I. Dahlan, H. M. Zwain, M. A. O. Seman, N. H. Baharuddin and M. R. Othman, Adsorption of brilliant green dye in aqueous medium using magnetic adsorbents prepared from rice husk ash, *AIP Conf. Proc.*, 2019, 2124.
89 S. N. Matussin, F. Khan, M. H. Harunsani, Y. M. Kim and M. M. Khan, Photocatalytic degradation of brilliant green and 4-nitrophenol using Ni-doped Gd(OH)3 nanorods, *Sci. Rep.*, 2024, **14**(1), 8269.